The mid Holocene sea-level change in the Arabian Gulf

Barbara Mauz[1,2], Mohammad Alsuwaidi[3], Zhixiong Shen[4], Daniele Mellini[5], Giorgio Spada[6], Sam J. Purkis[7]

[1] School of Environmental Sciences, University of Liverpool, Liverpool, L69 7ZT, UK
[2] Department of Environment and Biodiversity, University of Salzburg, Salzburg, 5020, Austria
[3] Khalifa University, Department of Earth Sciences, Abu Dhabi, United Arab Emirates
[4] Department of Marine Science, Coastal Carolina University, SC 29528, USA
[5] Sezione di Sismologia e Tettonofisica (Roma I), Roma, 00143, Italy
6
7

Abstract

The mid-Holocene sea-level highstand is a well-known phenomenon in sea-level science, yet the knowledge on the highstand's spatial and temporal distribution remains incomplete. Here we study the southwest coast of the Arabian-Persian Gulf where a mid-Holocene sea-level highstand and subsequent sea-level fall may have occurred due to the Earth crustal response to meltwater load. Sea-level indicators were established using standard facies analysis and error calculations and subsequently constrained through glacial-isostatic adjustment (GIA) modelling and though procedures based on Gaussian Process and exponential decay analysis. These analyses allowed to identify the highstand at 1.6±0.4 m occurring 6.7 – 6.0 ka, in excellent agreement with GIA model results. The subsequent shoreline migration followed the geophysical constraint by prograding in line with the sea-level fall until around 3 ka when the strength of the external control weakened and internal processes, in particular sediment binding through microbial activity, started controlling the size of the accommodation space.

1 Introduction

The Holocene sea-level history is of interest because, for this time period, high-resolution data are available to reliably constrain geophysical models which describe the response of the Earth and the oceans to deglaciation. From both geophysical models and proxy data, it is well-known that the sea level in the Holocene rose above its modern level in certain coastal areas, after the melting of the biggest ice sheet (Laurentide) has ceased (Mitrovica and Peltier, 1991). This was attributed to the interplay between equatorial ocean syphoning and 'continental levering' (Mitrovica and Milne 2002). The geophysical mechanisms controlling the mid Holocene sea-level highstand are thus well-understood, but our knowledge on the highstand's spatial and temporal distribution remains incomplete (Woodroff and Horton, 2005). Here we aim to contribute to this incomplete knowledge

by investigating the southwest coast of the Persian-Arabian Gulf (hereafter "Arabian Gulf'). The coast of the Arabian Gulf has been studied extensively (e.g., Kendall and Alsharhan 2011) and all these studies agreed that a sea-level highstand must have occurred at around 6 ka (e.g., Lokier et al., 2015; Parker et al., 2020; Engel et al., 2021). Yet, the exact elevation of the highstand and the response of the coast to the subsequent sea-level fall is still unclear. Our objective is therefore to close this data gap by establishing sea-level proxy data for the shoreline position. This position is likely controlled by the Earth's crustal response to meltwater load as well as by local processes such as carbonate productivity, hydrodynamically induced erosion and geometry of accommodation space. If the spatio-temporal distribution of the proxy data is mainly externally controlled, the proxies reflect the Arabian Gulf's crustal response to meltwater load. If the proxies do not follow the modelled response to the melting of ice sheets, then it can be assumed that internal controls dominate the indicative meaning of the proxies, hence the shoreline position. We show here that proxy data require additional analytical treatment to reliably quantify the geophysically-induced signal.

2 The study area

The Arabian Gulf (Fig. 1) is part of the Arabian plate characterised by topographic asymmetry with high elevations in the west and surface dipping to the east where the Gulf forms a foredeep basin dipping towards the north-eastern Zagros Mountains. The plate's crust and, most likely also the lithospheric mantle, thickens to the east leading to an overall lithospheric thickness of ~160 km beneath the foredeep basin of the Gulf (Stern and Johnson, 2010). The gulf is an epicontinental sea separated from the Indian Ocean by the Strait of Hormuz where the water depth of the sill is ~80 m (Bower et al., 2000). The annual mean water volume transport at the Strait is relatively small (Bower et al., 2000) suggesting that the flooding of the basin in deglacial times occurred at a slow pace. The average water depth in the Gulf is today 35 m and reaches around 100 m near the entrance at the Strait. The sea-water current in the Gulf is anti-clockwise from the Strait of Hormuz with highest salinity (dense water) in the southwest (Alsharhan and Kendall 2003).

Sites suitable for studying the Holocene sea-level history are situated on the western and southern coast of the Gulf which exhibits tectonic quiescence and absence of sediment disturbances such as compaction and unsuitable sedimentation rate. We investigated (1) Al Khidayrah and (2) Mussafah Channel and studied literature on (3) North Qatar and (4) Ghagha island (Fig. 1).

On the SW coast, diurnal and mixed tidal regimes dominate with tidal ranges of 1.0 - 1.5 m in protected zones (e.g., lagoon) and ~2.5 m on open coasts (Alsharhan and Kendall, 2003). Mean

spring tide is 1.1 m and mean neap tide is 0.75 m modified by diurnal inequality and occasional strong winds.

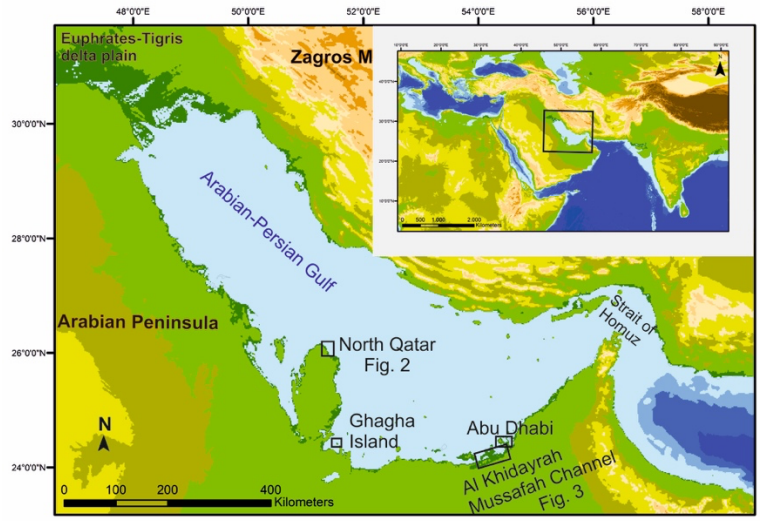

Fig. 1. The Arabian-Persian Gulf and location of studied sites. Map downloaded from ETOPO Global relief model doi:10.7289/V5C8276M.

2.1 Coastal sediments

The study area is part of the Arabian Gulf's homoclinal carbonate ramp (Read 1985), the geometry and topography of which is a result of the eastward dipping foredeep basin and the carbonate factory. This factory operates year-round with 10-100 mm/a sedimentation rate (Reijmer, 2021) resulting in a flat-topped platform geometry with a steep slope at ~40 m water depth (Park, 2011). In the protected coastal zones behind barrier islands, the typical lateral sedimentary succession of the inner ramp is composed of low-lying sabkhas and their evaporitic components (e.g., anhydrite) in places overlain by beach ridges; this is seaward followed by algal and microbial mats, mangrove mud, carbonate sand and silt and hardground (see Figs S1 and S2 for upper intertidal and hardground). On the open coast, the sabkha is seaward followed by oolitic or skeletal sand and coral reefs (Purkis and Riegl, 2005). The coast is therefore an evaporitic factory gradually transforming seaward into a carbonate factory where seasonally blowing strong winds influence the distribution of the carbonate facies.

The carbonate factory is dominated by bio-chemically induced precipitation of mud and peloids and by skeletal components (calcareous algae, foraminifera, bryozoans). On the inner ramp, benthic microbial communities typically dominated by cyanobacteria dominate the factory. They secrete extracellular polymeric substances (biofilm) which trap and bind sediment and organic matter (Suarez-Gonzales et al. 2019). The mats are biostabilisers, thereby contributing to the factory's capacity to build fast-prograding sediment bodies (Reijmer, 2021, Williams et al., 2011). Besides

these mats, the second important component of the inner ramp is hardground which forms in the inter- to subtidal through precipitation of carbonate minerals on the surface of carbonate particles supported by algal filaments (e.g., Christ et al., 2015; Ge et al., 2020). The flat pavement formed by hardground is widespread in water depth <2 m but also occurs in deeper water where it provides the ground for corals to settle and grow (Purkis et al., 2011). Carbonate sand and silt, represented by grain- and packstone facies is the typical product of the factory filling tidal creeks and channels as well as pools between microbial mats. The unconsolidated material is swept by tidal currents, hence transported in and out of the inner ramp. On the Gulf's arid coast, beachrock forms in the supratidal zone through evaporation of sea-water spray and episodically occurring rainwater in the pores of the carbonate sand.

The spatial distribution of the nearshore facies relevant for sea-level reconstruction is not the same everywhere but exhibits variable relationships to water depth. The patterns displayed in Figs 2 and 3 exemplify the ongoing debate about facies distribution on carbonate platforms: the distribution may follow patterns such as belts (e.g., Burchette and Wright, 1992), mosaics (Wright and Burgess, 2005), scale-invariant fractals (Schlager, 2004; Purkis et al., 2005) or it follows a power-law relationship (Purkis et al., 2005).

2.2 The Holocene sea-level highstand in the Arabian Gulf

The carbonate ramp and in particular the coast around Abu Dhabi was studied frequently (e.g., Evans, 2011; Shinn, 2011; Kirkham and Evans, 2020) and in great detail (e.g., Purkis et al., 2005; Strohmenger et al., 2011;. All these studies agreed that a mid-Holocene sea-level highstand occurred at 2-3 m (Strohmenger et al., 2010) or at ca 1 m (Lokier et al., 2015). For the Euphrates-Tigris delta Aqrawi (2001) found a mid-Holocene marine intrusion lasting around 2 ka. For the western coast Parker et al. (2020) found the highstand at ca 2.4 m occurring around 6.9 ka. For the north coast of the Qatar Peninsula Rivers et al. (2020) found the highstand at 1.6 m lasting around 2 ka (7-5 ka). Lambeck (1996) studied the Holocene shoreline migration using his glacial-isostatic adjustment (GIA) model and predicted a 3.5 m highstand occurring on the SW-coast of the Gulf.

3 Methods

The methodological approach assumes that the sea-level indicator carries the signature of externally and internally induced processes. The external control is exerted by GIA-induced processes and the internal control is induced by local processes such as hydrodynamics, carbonate productivity and microbial activity. The indicator provides proxy data for the spatio-temporal distribution of the shoreline position. The indicator is converted to a true sea-level index point (SLIP) through (i)

accurate and precise elevation data including error estimation, (ii) calibrated radiocarbon age and (iii) detailed lateral and vertical facies description to infer indicative meaning and indicative range of the dated deposit (for details see supplement).

3.1 Field survey and elevation

To survey modern coastal facies, field work targeted artificial outcrops ('SH' in Fig. 3A inset) at the modern shoreline. To relate this with buried coastal facies pits were dug in beach ridges. All sites including the Mussafah Channel (MC) site (Fig. 3; Kirkham, 1998; Strohmenger et al., 2010) were measured using dGPS levelled to benchmark ID 3197 (Abu Dhabi). Sampling focused on hardgrounds for thin section analysis and on intertidal carbonate sand for XRF and radiocarbon analyses. In a subsequent field visit data and the facies interpretation was tested and verified.

3.2 Facies analysis

To determine the indicative meaning of each sea-level indicator the modern analogue of facies distribution was established. For this purpose, results from field survey and logging and from x-ray fluorescence (XRF) analysis (see supplement for details) were compared and complemented with data from literature for the purpose of facies description. Nearshore facies distribution was mapped from Google Earth images and the geological map of Alsharhan and Kendall (2003).

3.3 GIA modelling

To quantify the external control on sea-level indicators, past sea-level history was modelled by obtaining a set of high-resolution numerical solutions of the Sea-Level Equation using the SELEN4 solver (Spada and Melini, 2019). Each numerical solution was computed on a global icosahedral grid with spacing of ~40 km. It accounts for spectral terms up to harmonic degree L=512 corresponding to a wavelength of ~78 km on the Earth's surface. The boundary conditions for paleo-topography are prescribed through the ETOPO1 global topographic model (Amante and Eakins, 2009), integrated with the Bedmap2 relief (Fretwell et al., 2003) of the Antarctic region. Three global GIA models were used, i.e., ICE-6G (Peltier et al., 2015), ICE-7G (Roy and Peltier, 2015, 2017) and one of the models progressively developed by the Kurt Lambeck group at the Australian National University (ANU, e.g., Lambeck et al., 2003). For each model run the nominal rheological profile and a modified profile was implemented where the modified profile used a lithospheric thickness (LT) of 160 km indicated by Stern and Johnson (2010) for the eastern portion of the Arabian plate.

3.4 Modelling proxy data

Most of the SLIPs established cover the sea-level fall subsequent to the mid-Holocene highstand. This fall should be controlled by the crustal response to water load (Mitrovica and Milne 2002) with minor contribution of additional meltwater. If SLIPs are mainly externally controlled, they follow the GIA prediction in terms of time and elevation. If SLIPs are mainly internally controlled their spatio-temporal distribution deviates from the GIA prediction. To assess this, all those proxy data that indicate sea-level fall were fitted using the exponential decay function of the form $y=a*e^{(-x/t)}+y_0$ where a and y_0 stand for amplitude and offset, respectively, and 1/t represents the decay rate. This type of decay function is prescribed by the shape of the sea-level curves obtained from the GIA models for the period ca 6-0 ka when sea level falls (Fig. S2). In addition, the proxy-data distribution was modelled using a Gaussian process (GP) model for the period 4-0 ka. The GP model runs with seven hyperparameters (prior standard deviations) representing fast (decadal scale) and slow (centennial scale) changes of global sea level, fast and slow changes of sea level on local and regional scales, and a regionally varying linear hyperparameter for a GIA process deduced from ICE 5G-VM2-90. For details of the model see Kemp et al. (2018). After a test run for individual sites which returned insignificant difference between sites, the SLIP data were combined to one virtual site.

3.5 Sea level and shoreline analysis

To assess the internal control on sea-level indicators the rate of sea-level fall was compared with the rate of shoreline progradation. It is expected that the shoreline migrates at a rate smaller than the size of the accommodation space changes, because the year-round operating carbonate factory remains unaffected by the geophysical process governing the sea-level change. The shoreline migration is calculated using the well-defined location of the MC site (Fig. 3A) which is 8 km away from the present-day mean shoreline (Kirkham, 1998). The slope angle of the inner ramp is 0.07° (Lokier et al 2018) or, in some areas, it is 0.05° to 0.06° or 0.48° and 0.53° (Court et al., 2017; see also 3D model of this ramp in Purkis et al., 2005). Using a linear regression line with *x* being the distance between the MC site and the modern shoreline and the slope resulting from tan(α), where α=0.07° or α=0.04°, the shoreline progradation is calculated for the period 6.7 – 0 ka. The approach assumes that over the small temporal scale of interest here, the slope angle at a given location is constant. The rate of sea-level change was deduced from the exponential fit of the proxy data.

3.7 Uncertainties

The generation of sea-level data includes uncertainties arising from measurements (elevation, dating) and models, and also from facies analysis. The latter represents the uncertainty of water-depth attribution to a dated sea-level indicator. For biotic indicators (e.g., corals) this is the living

range and, for bio-chemically induced deposits, it is the water-depth range of a given facies. Because the carbonate factory studied here is a bio-chemical system with variable spatial distribution of biostabilisers, the deterministic approach 'one facies, one water depth', hence indicative range, is likely inappropriate to capture the true indicative range. Equally, the summing in quadrature of error terms seems insufficient to capture the true variability of the water depth. On the other hand, including all possible water depths into the error term of a given facies and propagating this alongside other errors, the resulting effective uncertainty would render the associated value meaningless. Here, we use the standard procedure of error calculation for individual data points (Hijma et al., 2015), but calculate the uncertainty of the highstand elevation from the 95% confidence level (CL) of the exponential fit (see Fig. S3 for CL).

4 Results

4.1 Sedimentary facies and indicative meaning

On the barrier island coast (Abu Dhabi) the sedimentary succession relevant for Holocene sea-level assessment starts with microbial mat or hardground (Fig. S4A and C) situated around 1– 2 m above modern sea level. On the north Qatar coast it starts with intertidal carbonate sand or reef mounds overlying Eocene bedrock (Fig. S4B). It follows 1-2 m thick carbonate fine sand represented by intertidal skeletal grainstone, packstone or laminated fine sand characterised by Ca/Si ~20 (Fig. S5A). The supratidal is represented by bioclastic sand, anhydrite and halite- or gypsum crust reflected by high calcium and sulphate percentages in the sediment (Fig. S5B). On the coast behind barrier islands sediment successions are dominated by tidal channel facies (Fig. S4C). The Holocene flooding surface is carved into bedrock (Qatar) or it is a hardground (Abu Dhabi) characterised by granular texture (for details of hardground facies see Table S1). On Ghagha island the succession is composed of Neogene limestone overlain by bioclastic sand in places cemented to beachrock.

The modern coastal sedimentary environment shows a facies distribution of evaporitic anhydrite or halite-gypsum mud and bioclastic sand in the supratidal, carbonate sand, algal- and microbial mats, hardground and reef mounds in the inter- to subtidal. Modern facies distribution appears to be random on the open coasts of north Qatar (Fig. 2) and appears to follow belts on small scale (Fig. 3).

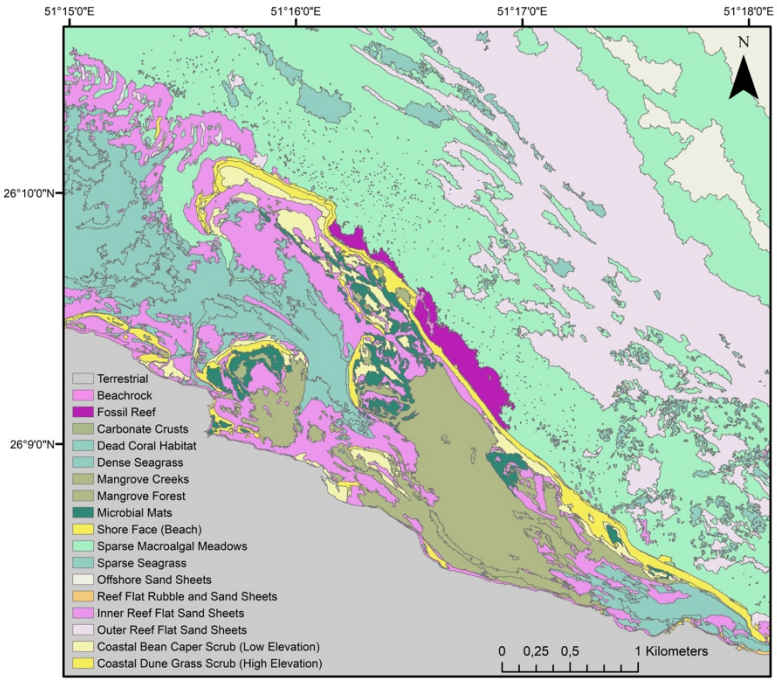

Fig. 2. The modern facies distribution on the tidal flat off north Qatar (modified from Purkis et al., 2017).

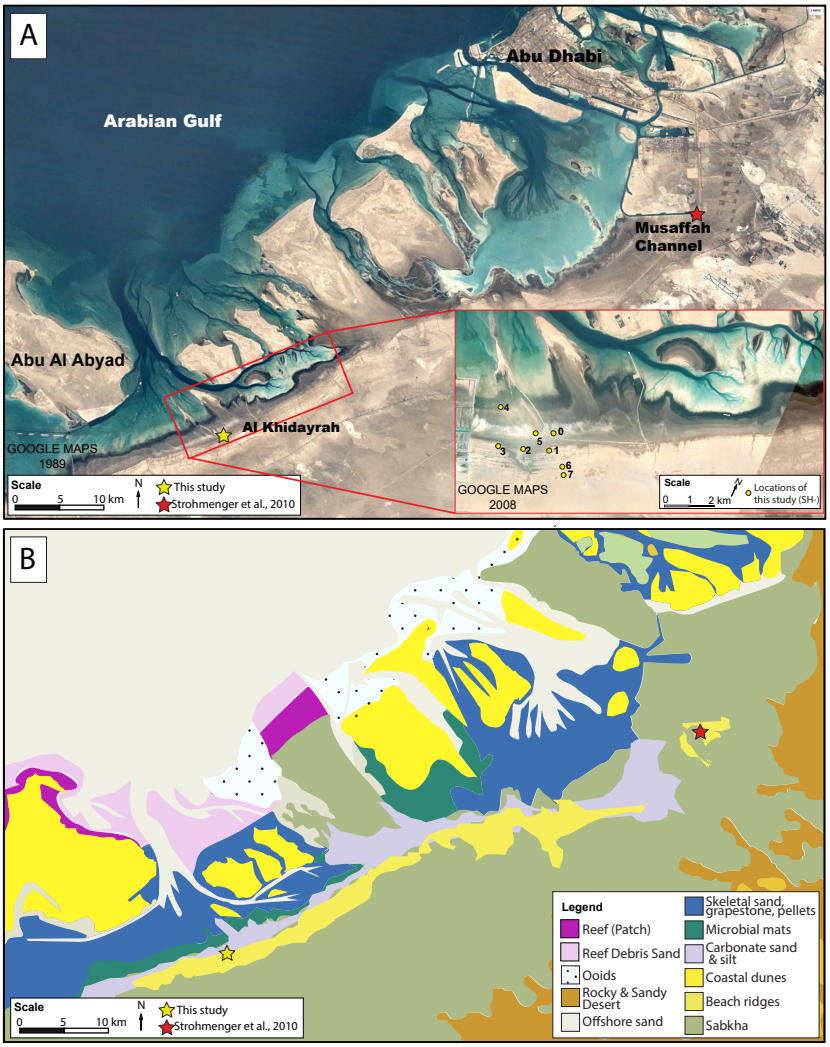

Fig. 3. A - The modern coast west of Abu Dhabi and location of studied sites; B - The modern facies distribution (modified after Alsharhan and Kendall, 2003).

235

4.2 Proxy data

On the basis of lateral and vertical facies distribution the modern analogue facies model (Fig. 4) provides the relative water depth of facies, hence indicative meaning and range of sea-level indicators.

240

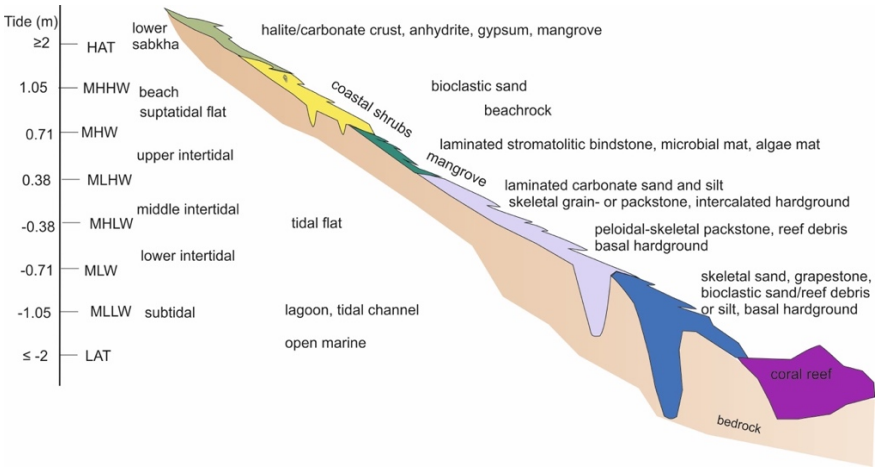

Fig. 4. Concept of facies distribution deduced from the modern analogue displayed in Figs 2 and 3 and from literature (Alsharhan and Kendall, 2003; Strohmenger et al., 2011).

The modern analogue of facies distribution (Figs 2, 3, 4) together with the established requirements for sea-level indicators result in 22 proxy data points where 16 are SLIPs, 4 are terrestrial limiting and 2 are marine limiting data points (Table 1; for details of data see supplement).

Table 1. Proxy data generated in this study. Reference water level is mean sea level for all samples. For details see supplement.

Site	Sample	Lat	Long	Elevation (m)	Age (cal BP)	IR (m)	Palaeo mean sea level	Indicator	Reference
Al Khidayrah	SH1R	24.11	54.06	1.35±0.03	2.87±0.35	0.38±0.19	0.97±0.19	Carb sand; SLIP	This study
Al Khidayrah	SH2R	24.11	54.05	1.35±0.03	2.79±0.37	0.38±0.19	0.97±0.19	Carb sand; SLIP	This study
Al Khidayrah	SH7L	24.10	54.07	2.20±0.04	6.26±0.37	1.00±0.50	1.20±0.50	Beach ridge; terr limiting	This study
Al Khidayrah	SH7U	24.10	54.07	2.50±0.04	5.67±0.38	1.40±0.70	1.10±0.70	Beach ridge; terr limiting	This study
Al Khidayrah	SH6U	24.10	54.06	2.26±0.03	4.26±0.42	1.40±0.70	0.86±0.70	Beach ridge; terr limiting	This study
Al Khidayrah	SH6L	24.10	54.06	1.94±0.03	4.58±0.42	1.00±0.50	0.94±0.50	Beach ridge; terr limiting	This study
Mussafah	MC1-4	24.31	55.29	2.15±0.03	6.35±0.41	0.55±0.27	1.61±0.27	Microbial mat; SLIP	Strohmenger et al., 2010

Mussafah	MC2-2	24.31	55.29	2.22±0.03	6.80±0.43	0.55±0.27	1.68±0.27	Microbial mat; SLIP	Strohmenger et al., 2010
Mussafah	MC3A-2	24.31	55.29	1.75±0.03	6.30±0.42	0.55±0.27	1.21±0.27	Microbial mat; SLIP	Strohmenger et al., 2010
Mussafah	MC3A-7	24.31	55.29	2.65±0.03	5.78±0.46	0.70±0.35	1.95±0.35	Hardground; SLIP	Strohmenger et al., 2010
Mussafah	MC4-2	24.31	55.29	1.90±0.03	6.79±0.43	0.55±0.27	1.36±0.27	Microbial mat; SLIP	Strohmenger et al., 2010
North Qatar	C1-1	26.15	51.27	0.13±0.02	5.81±0.12	1.20±0.60	1.33±0.60	Carb sand; SLIP	Rivers et al., 2020
Al Ruwais	C4-1	26.14	51.27	-0.13±0.02	6.06±0.15	1.80±0.90	1.07±0.90	Carb sand; SLIP	Rivers et al., 2020
Al Ruwais	C4-2	26.14	51.27	0.02±0.02	6.73±0.16	1.80±0.90	1.22±0.90	Carb sand; SLIP	Rivers et al., 2020
Al Ruwais	C4-3	26.14	51.27	0.82±0.02	5.75±0.14	1.80±0.90	2.02±0.90	Carb sand; SLIP	Rivers et al., 2020
Al Ruwais	C4-4	26.14	51.27	0.84±0.02	5.98±0.17	1.80±0.90	2.04±0.90	Carb sand; SLIP	Rivers et al., 2020
Um Tays Island	C5-1	26.16	51.28	-2.84±0.02	3.90±0.17	2.50±1.25	-1.64±1.25	Reef; marine lim	Rivers et al., 2020
Um Tays Island	C5-2	26.16	51.28	-2.60±0.02	3.66±0.16	2.50±1.25	-1.40±1.25	Reef; marine lim	Rivers et al., 2020
Ghagha island	G03	24.41	51.55	2.43±0.24	6.31±0.11	1.50±0.75	1.55±0.79	Beachrock; SLIP	Arhan et al., 2020
Ghagha Island	Ge2	24.41	51.55	2.87±0.0.29	5.88±0.14	1.00±0.50	1.99±0.58	Beachrock; SLIP	Arhan et al., 2020
Ghagha Island	Ge1	24.41	51.55	1.67±0.17	3.30±0.26	1.00±0.50	0.79±0.53	Beachrock; SLIP	Arhan et al., 2020
Khawr Qantu	Site01-B39	24.12	54.03	-0.0205± 0.0008	1.24±0.35	0.55±0.27	0.53±0.27	Microbial mat; SLIP	Lokier and Steuber, 2008
Khawr Qantu	Site10-S143	24.12	54.01	-0.275± 0.011	0.46±0.31	0.55±0.27	0.27±0.27	Microbial mat; SLIP	Lokier and Steuber, 2008

4.3 GIA

The sea-level curves simulated by the ICE-7G and ANU models are similar in terms of trend and timing of the sea-level highstand (Fig. 5). The ICE-7G model predicts a highstand that is around 0.8 m higher than the one predicted by ANU. For the time 6-0 ka both curves follow a single exponential decay with ICE-7G being almost identical (χ^2_{red}=0.00036) to this mathematical description (Fig. S2).

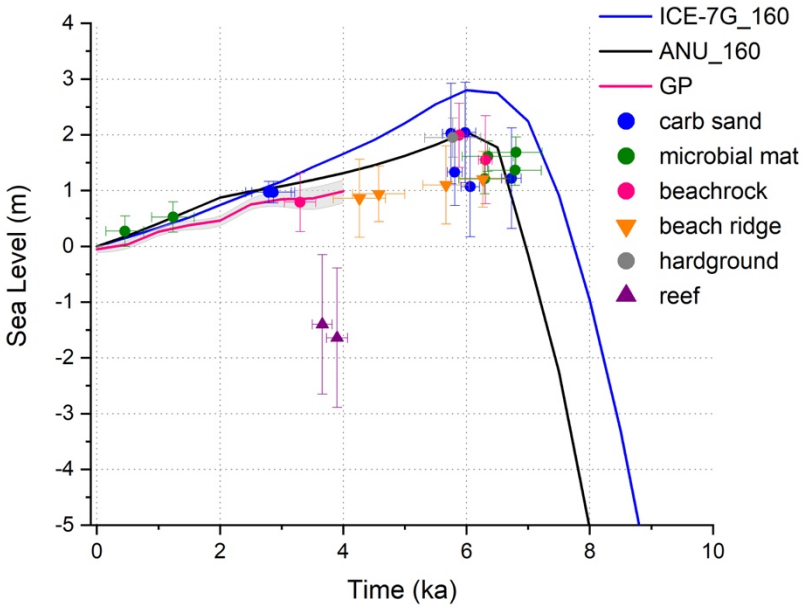

Fig. 5. Sea-level curves predicted by ICE-7G and ANU models (LT=160 km) and by the GP model compared to all proxy data.

4.4 Proxy data and model results

The sediment succession in the MC site (Fig. S4C) indicate increasing water depth between microbial mat and upper hardground. The mid-Holocene microbial mats are therefore part of the transgressive phase with the maximum transgression surface indicated by the upper hardground. All other proxies reflect the falling sea level occurring subsequent to the highstand. Proxy data derived from intertidal carbonate sand, beachrock, microbial mats and hardground deliver variable elevations but are consistent within error margins. Proxy data derived from beach ridges plot consistently around 0.7 m and those derived from the reef plot around 2 m below the predicted elevation. In the MC site the highstand is indicated by the hardground at 2.0±0.4 m and 5.8±0.5 ka (Fig. S4C).

The curve resulting from the exponential fit of the proxy data (Fig. S3; except marine limiting points and mid-Holocene microbial mats) is flat and curved compared to the curves derived from the GIA models (Fig. 6). The curved shape is dictated by the data points representing the period 3-0 ka. The exp proxy curve indicates the highstand to occur at 1.6±0.4 m around 6.7 ka. The ANU model indicate the highstand at 2.0 m and the ICE-7G predicts the highstand to occur at 2.8 m. Both GIA models predict the highstand for the time around 6 ka. The GP-modelled curve falls from around 1 m to zero, which is the trend indicated by the proxy data. The shape of the curve follows the global sea-level function implemented in the GP model (Fig. S8B).

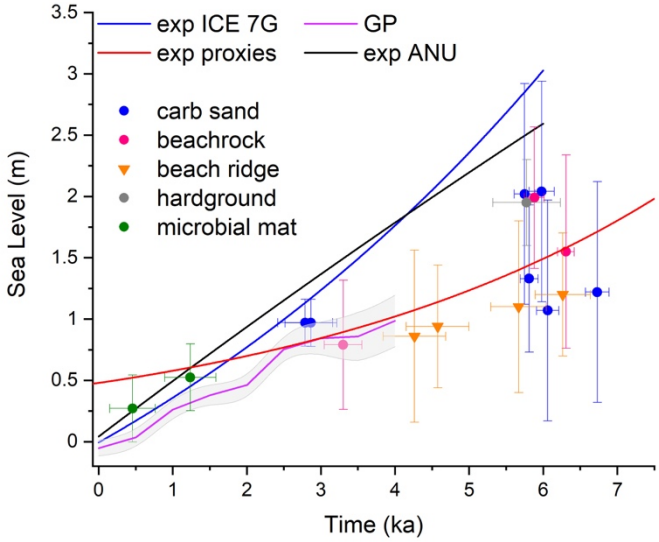

Fig. 6. The curves resulting from the exponential decay fit of ICE-7G (blue), ANU (black) and proxy data (red; data points representing transgression excluded). Gaussian Process (GP) model curve (purple) and proxy data are also plotted. For details of fits see Figs S2 and S3.

4.5 Sea level and shoreline

On the inner carbonate ramp the shoreline prograded since 6.7 ka downslope between around 10 m (slope angle 0.07°) and around 6 m (slope angle 0.04°) (Fig. 7). The sea level fell at the same time from 1.6 m to zero meter. Where the slope angle is 0.07° the shoreline migrated almost in pace with the sea-level; on slopes with <0.07° angles the shoreline's progradation is reduced.

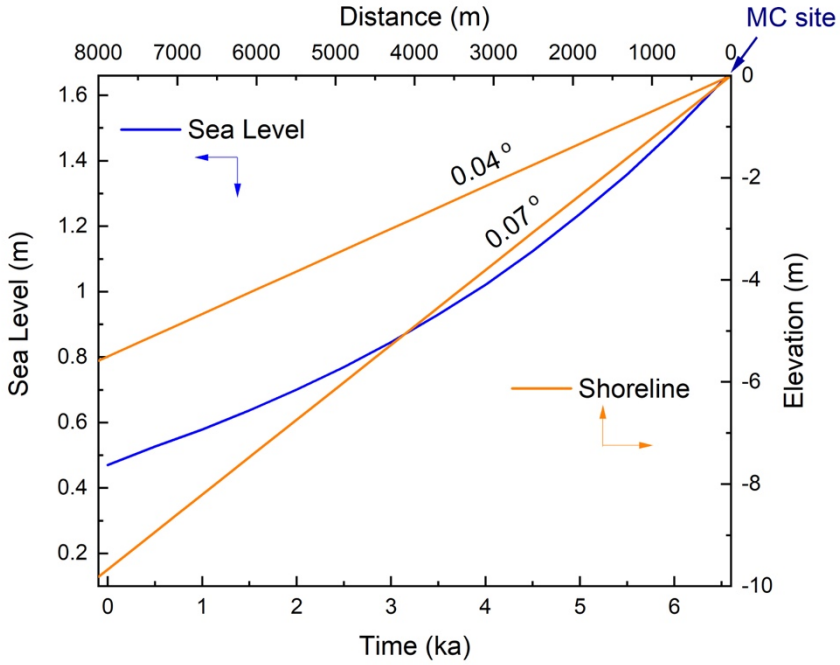

Fig. 7. The sea-level fall (blue line) and the shoreline progradation line (orange line) since the mid Holocene calculated for the MC site. At 6.7 ka the shoreline is at 0 m elevation at the MC site and then migrates seaward over a distance of 8 km following the falling sea level.

5 Discussion

5.1 Indicative meaning and quality of proxy data

In this study sea-level indicators selected for the purpose of sea-level reconstruction were intertidal microbial mats, hardground and carbonate sand, subtidal coral reef and supratidal beachrock and beach ridges. The N-Qatar coast sea-level indicators were derived from intertidal carbonate sand and *in situ* coral remains (Rivers et al., 2020). With a tidal range of 1.1 m (up to 2.3 m) the flooding surface must be -1 m at 4 ka to reconstruct a highstand of approximately 2 m, but the surface is at -3 m and, consequently, the reef-derived proxy data plot below the expected sea-level. It is possible that the Eocene bedrock surface was carved during the LGM lowstand and was colonised during deglacial sea-level rise by a coral assemblage for which the bedrock surface was situated within its living range (e.g., Riegl and Purkis, 2012 for living range of corals). For the Ghagha island coast sea-level indicators were derived from beachrock (Arhan et al., 2020) which is a reliable indicator for the supratidal zone due to the immediate lithification of the beach sand. For the Abu Dhabi barrier island coast intertidal microbial mats, carbonate sand and hardground are indicators of variable reliability. Microbial mats seem to be more linearly related to water depth in protected zones behind barrier islands (Fig. 2) but on the open coast east of Abu Dhabi they can colonise sandy substrates almost everywhere in the intertidal to upper subtidal zone (Purkis et al., 2005). It appears that the microbial mats grow to a thickness that can withstand high-energy waves and currents in protected zones where they have time to the develop the biofilm (Mariotti and Fagherazzi, 2012). Thus, on the inner carbonate ramp it is the absence of high energy rather than the water depth that controls the occurrence of the mats. Carbonate sand is mostly unconsolidated, hence mobile and easily swept by tidal currents. In fact, the variable vertical succession of the two key stratigraphic facies, i.e., hardground and microbial mat (see Fig. S4 and Strohmenger et al., 2011) indicates a complex spatial relationship between facies. This is not reflected in the modern analogue facies model (Fig. 4) which is suggestive of a belt-shaped concept where facies is parallel to the shoreline and linearly related to water depth. The question is, therefore, whether small sea-level changes can trigger facies-belt migration or trigger extension or reduction of belts where the mean water depth of individual facies belts remains constant. Also, the water depth may be variable in places owing to the variable tides (semidiurnal to diurnal with diurnal inequalities) and to the strong winds which

affect the arrival time of high and low tides and the tidal currents. The nearshore facies distribution on a carbonate ramp has been described as a mosaic (Purkis et al., 2005; Wright and Burgess, 2005; Kendall and Alsharhan, 2011) rather than belt-shaped, and this clearly impairs rigorous quantification of water depth. Moreover, some of our sea-level proxy data are obtained from the protected coast behind barriers where the facies are dominated by tidal channel deposits, indicating substantial lateral movement of unconsolidated sand including the destroying of earlier facies successions. On the other hand, the reconstructed modern analogue in Fig. 4 is a result of a decrease in accommodation space due to sea-level fall, and this is what we reconstruct in this study. We can say that our sea-level proxies determined on the basis of the modern analogue are uncertain observations of the true shoreline position. The quantitative uncertainty associated with the observation is then not noise resulting from measurements, but reflects our incomplete understanding of the quantified system.

5.2 GIA models

The sea-level curves obtained from the two ICE models (ICE-6G and ICE-7G) are almost identical (Fig. S6) despite the different viscosity profiles (Fig. S7) employed in each model. Moreover, the output of the ICE models remain identical also when the regional-scale lithospheric thickness of 160 km is used instead of the nominal value (90 km). Only the higher viscosity profile for the lower mantle seem to affect the model output as indicated by the curve obtained from ANU (Fig. 5) where the highstand is around 0.8 m lower than the one predicted by the ICE models. Thus, assuming a thick lithosphere of 160 km and a high lower mantle viscosity brings the elevation of the highstand from around 3 m closer to the proxy data which suggest less than 2 m. ANU and ICE are also different in terms of the eustatic functions where ANU implements continuous melting of the Antarctic until 2 ka and the ICE models assume all melting has ended by 6 ka (Fig. S8A). This should affect the modelled water load in the gulf after 6 ka, hence the shape of the simulated curve. However, the rate of sea-level change is almost identical in both GIA models for the time 6-0 ka (Fig. S9) and thus, any additional meltwater injected after 6 ka does not affect the crustal response of the eastern Arabian plate. Lambeck (1996) postulated a 3.5 m sea level for the coast between Qatar and Abu Dhabi. Without knowing all details of model parametrisation, we can only speculate that the around 1.5 m difference to our model result is owed to the rheological profile and, certainly also, to the numerical solution of the models. The timing of the highstand itself and the timing of the subsequent sea-level fall is almost identical in all predictions and some 100 years later than indicated by the proxies.

5.3 Proxy data modelling results

With the uncertain shoreline observation in mind, it cannot be assumed that individual proxies provide a SLIP, but the assemblage of proxy data derived from the same coast experiencing the same sea-level history should deliver reliable information, subject to analytical procedures that account for the underlying processes. We have selected two analytical procedures: Gaussian Process (GP) and exponential decay. The first employs a spatio-temporal statistical analysis to decompose the local dataset of sea-level change in addition to a global one, and the second follows the geophysical constraints.

The GP model captures the trend of the proxy data and suggests that its key assumption, that is the normal distribution of data, is valid despite the different context of the proxies themselves. This is an astonishing result given the uncertain observation provided by individual sea-level indicators. Both the GP-modelled curve and the proxy curve derived from the exponential-decay model (exp proxy, Fig. 6) plot below the GIA curves (exp ICE-7G and exp ANU). This confirms the sea-level fall indicated by the proxy data which is a little lesser than the one indicated by the GIA-curves (Fig. 6). The exp proxy curve seem to describe the data well for the early period of the sea-level fall (7-3 ka) but less so for the late Holocene when the external control on shoreline migration tapers off. The difference between proxy data, GP result and GIA prediction is therefore solely caused by the elevation difference of the highstand and that is 0.3-0.5 m. This difference translates to a difference in shoreline position along the slope of 250-400 m. With the width of the modern microbial mat belt being 150-800 m (Court et al., 2017) and the ability of the mats to adjust quickly to a changing accommodation space (e.g., Wu et al., 2021), we can say that the global GIA models perfectly approximate the shoreline positions inferred from the proxy data.

5.4 Sea-level fall and shoreline migration

The comparison between sea level and shoreline should allow to qualitatively assess the influence of internal processes on the proxy data. The internal factors controlling the position of the shoreline are the slope angle (geometry) and the organisms which bind the sediment produced in the carbonate factory from where it is transported upslope onto the platform. The results indicate that the movement of shoreline is in line with the sea-level fall (Fig. 7), as long as the slope angle is 0.07°. This indicates that the inner ramp geometry was in equilibrium between reduction of accommodation space and sediment accumulation during the mid-late Holocene. This changed in the late Holocene when the external control on shoreline migration had decreased and, consequently, sediment supply started dominating the progradation rate. Where the slope angle is shallower, the shoreline migrated at a slower pace most probably owing to enhanced microbial activity (and therefore sediment stabilisation) on the tidal flat. We can therefore say that the

shoreline migration is controlled by external forcing as long as this forcing is strong enough to exceed the impact of internal processes on the accommodation space.

5.5 Magnitude and timing of the highstand

Following the analysis of the proxy data the sea-level highstand was at 1.6 ± 0.4 m with negligible difference to the elevations indicated by the GIA models. The highstand lasted ~6.7 – 6.0 ka as also indicated by our models. The high precision of radiocarbon dating notwithstanding, we prefer to give a "circa" timing because different calibration curves and reservoir ages (ΔR) form the basis of the ages used in this study. The chronology of the GIA models is based on IntCal09 or Marine09 with a constant reservoir age correction of 405 years (Reimer et al., 2009). Rivers et al. (2020) and Arhan et al. (2020) used Marine13 (Reimer et al., 2013) combined with ΔR=180 ± 53 (Southon et al., 2002). The reservoir age alone leads to >200 years difference in the timing of the highstand (see also Lindauer et al., 2017 for changes of ΔR during historical times).

6 Conclusions

It is a challenge to apply a deterministic approach to a carbonate ramp environment for which facies distribution is debated to exhibit linear, random/stochastic and fractal relationships to water depth. Biostabilisers as well as geometry of tidal flats with respect to storm and tidal waves play a major role in shaping the accommodation space of sea-level indicators. Nonetheless, the shoreline followed the sea-level trend clearly and changed its migration only when the strength of the geophysical process weakened. This, in addition to the excellent agreement between results from proxy data analysis and GIA models, provide confidence in current methodology of sea-level science.

Acknowledgements

BM and MA thank Thomas Steuber (Khalifa University) for discussing details of slope profiles and shoreline migration. Sara Stuecker (University of Salzburg) helped with producing GIS maps. BM gratefully acknowledges Peter Burgess (University of Liverpool) for stimulating discussions on carbonate facies.

Author contribution

BM designed the research and wrote the manuscript. BM and MA conducted the field work and MA analysed samples and supported facies description and mapping. ZS conducted the GP modelling work. DM and GS conducted the GIA modelling work. SJP supported facies description and mapping. All authors contributed to the writing of the text.

References

Alsharhan, A.S. and Kendall, C.G.St.C. (2003). Holocene coastal carbonates and evaporites of the southern Arabian Gulf and their ancient analogues. *Earth-Science Reviews* 61, 191–243, doi:10.1016/S0012-8252(02)00110-1.

Amante and Eakins, 2009

Aqrawi, A.A.M. (2001). Stratigraphic signatures of climatic change during the Holocene evolution of the Tigris–Euphrates delta, lower Mesopotamia. *Global and Planetary Change* 28, 267–283, PII: S0921-8181Ž00.00078-3

Arhan, D., Paplopoulos, K. and Fouache, É. (2020). Holocene relative sea-level variations and archeological implications, Abu Dhabi western region, United Arab Emirates. Arabian Journal of Geosciences 13, 254, https://doi.org/10.1007/s12517-020-5155-9

Bower, A.S., Hunt, H.D. and Price, J.F., (2000). Character and dynamics of the Red Sea and Persian Gulf outflows. JGR 105(C3), 6387-6414.

Christ, N., Immenhauser, A., Wood, R.A., Darwich, K. and Niedermayr, A., 2015. Petrography and environmental controls on the formation of Phanerozoic marine carbonate hardgrounds. Earth-Science Reviews 151, 176-226, http://dx.doi.org/10.1016/j.earscirev.2015.10.002.

Court, W.M., Paul, A., Lokier, S.W., 2017. The preservation potential of environmentally diagnostic sedimentary structures from a coastal sabkha. *Mar. Geol.* 386, 1–8, http://dx.doi.org/10.1016/j.margeo.2017.02.003

Engel, M., Strohmenger, C.J., Peis, K.T., Pint, A., Brill, D. and Bruckner, H.,2021. High-resolution facies analysis of a coastal sabkha in the eastern Gulf of Salwa (Qatar): A spatiotemporal reconstruction. Sedimentology, in press, doi:10.1111/SED.12938

Evans, G. 2011. An historical review of the Quaternary sedimentology of the Gulf (Arabian/Persian Gulf) and its geological impacts. I*nt. Assoc. Sedimentol. Spec. Publ*. 43, 13-44.

Fretwell et al 2003

Ge, Y., Lokier, S.W., Hoffmann, R., Pederson, C., Neuser, R.D., Immenhauser, A., 2020. Composite micrite envelopes in the lagoon of Abu Dhabi and their application for the recognition of ancient firm- to hardgrounds. Marine Geology 423, 106141, https://doi.org/10.1016/j.margeo.2020.106141.

Hijma, M.P., Engelhart, S.E., Tornqvist. T.E., Horton, B.P., Hu, P., Hill, D.F., 2015. A protocol for a geological sea-level database, in Shennan, I. et al (eds), Handbook of sea-level research, Wiley, 536-556.

Kemp, A.C., Wright, A.J., Edwards, R.J., Barnett, R.L., Brain, M.J., Kopp, R.E., Cahill, N., Horton, B.P., Charman, D.J., Hawkes, A.D., Hill, T.D., van de Plasshe, O., 2018. Relative sea-level change in Newfoundland, Canada during the past ~3000 years. QSR 201, 89-110, https://doi.org/10.1016/j.quascirev.2018.10.012.

Kendall, C.G.St.C. and Alsharhan, A.S. (eds), 2011. Quaternary carbonate and evaporite sedimentary facies and their ancient analogues. *Int. Assoc. Sedimentol. Spec. Publ.* 43, Wiley-Blackwell.

Kirkham, A. and Evans, G. 2020. Carbonate sedimentation around Jebel Dhanna: models for parts of the buried Holocene sabkha sequences elsewhere along the Abu Dhabi coastline. Carbonates and Evaporites, 35, 24, https://doi.org/10.1007/s13146-020-00561-0.

Kirkham, A. (1998). A Quaternary proximal foreland ramp and its continental fringe, Arabian Gulf, U.A.E. In: Wright VP, Burchette TP (eds), Carbonate ramps, vol 149. Geological Society, London, Special Publication, pp 15–41.

Lambeck et al. 2003

Lambeck, K. (1996). Shoreline reconstruction for the Persian Gulf since the last glacial maximum. EPSL 142, 43-57.

Lindauer, S., Santos, G.M., Steinhof, A., Yousif, E., Phillips, C., Jasmin, S.A., Uerpmann, H.-P., Hinderer, M., 2017. The local marine reservoir effect at Kalba (UAE) between the Neolithic and Bronze Age: An indicator of sea level and climate changes. Quat Geochron 42, 105-116, http://dx.doi.org/10.1016/j.quageo.2017.09.003.

Lokier, S. and Steuber, T., 2008. Quantification of carbonate-ramp sedimentation and progradation rates for the late Holocene Abu Dhabi shoreline. JSR 78, 423-431, DOI: 10.2110/jsr.2008.049.

Lokier, S.W., Bateman, M.D., Larkin, N.R., Rye, P., Stewart, J.R., 2015. Late Quaternary sea-level changes of the Persian Gulf. Quat. Res. 84 (1), 69–81, http://dx.doi.org/10.1016/j.yqres.2015.04.007.

Lokier, S.W., Court, W.M., Onuma, T. and Paul, A. (2018). Implications of sea-level rise in a modern carbonate ramp setting. Geomorphology 304, 64–73, https://doi.org/10.1016/j.geomorph.2017.12.023.

Mariotti, G.and Fagherazzi, S. (2012). Modeling the effect of tides and waves on benthic biofilms. JOURNAL OF GEOPHYSICAL RESEARCH, VOL. 117, G04010, doi:10.1029/2012JG002064.

Mitrovica, J.X. and Milne, G.A., 2002. On the origin of late Holocene sea-level highstands within equatorial ocean basins. *Quaternary Science Reviews* 21, 2179–2190.

Mitrovica, J.X. and Peltier, W.R. (1991). On postglacial geoid subsidenc over the Equatorial oceans. J. Geophys. Res. 96, 20053-20071.

Park, R.K., 2011. The impact of sea-level change on ramp margin deposition: lessons from the Holocene sabkhas of Abu Dhabi, United Arab Emirates. Int. Assoc. Sedimentol. Spec. Publ. 43, 89-112.

Parker, A.G., Morley, M.W., Armitage, S.J., Engel, M., Parton, A., Preston, G.W., Russ, H., Drechsler, P. (2020). Palaeoenvironmental and sea level changes during the Holocene in eastern Saudi Arabia and their implications for Neolithic populations. *Quaternary Science Reviews* 249, 106618, https://doi.org/10.1016/j.quascirev.2020.106618.

Peltier, W.R., Argus, D.F. and Drummond, R. (2015). Space geodesy constrains ice age terminal deglaciation: The global ICE-6G_C (VM5a) model. J. Geophys. Res. Solid Earth, 120, 450–487, doi:10.1002/2014JB011176.

Purkis , S., Rivers, J., Strohmenger, C., Warren, C., Yousif, R., Ramirez, L. and Riegl, B. 2017. Complex interplay between depositional and petrophysical environments in Holocene tidal carbonates (Al Ruwais, Qatar). Sedimentology 64, 1646-1675, doi: 10.1111/sed.12368.

Purkis, S.J., Renegar, D.A., Riegl, B.M., 2011. The most temperature-adapted corals have an Achilles' Heel. Marine Pollution Bulletin 62, 246-250, doi:10.1016/j.marpolbul.2010.11.005.

Purkis, S.J., Riegl, B.M. and Andréfouët, S. 2005. Remote sensing of geomorphology and facies patters on a modern carbonate ramp (Arabian Gulf, Dubai, U.A.E.). Journal of Sedimentary Research, 2005, v. 75, 861–876, DOI: 10.2110/jsr.2005.067.

Read, J.F. (1985). Carbonate platform facies models. AAPG Bull. 69, 1-21.

Reijmer, J.J.G. (2021). Marine carbonate factories: Review and update. Sedimentology (2021) 68, 1729–1796, doi: 10.1111/sed.12878.

Reimer, P. J., Baillie, M. G., Bard, E., Bayliss, A., Beck, J. W., Blackwell, P. G., ... , Weyhenmeyer, C. E. (2009). IntCal09 and Marine09 radiocarbon age calibration curves, 0–50,000 years cal BP. *Radiocarbon 51*(4), 1111-1150.

Reimer, P.J., Bard, E., Bayliss, A., Beck, J.W., Blackwell, P.G., Bronk Ramsey, C., Buck, C.E., Cheng, H., Edwards, R.L., Friedrich, M., Grootes, P.M., Guilderson, T.P., Haflidason, H., Hajdas, I., Hatt e, C., Heaton, T.J., Hoffmann, D.L., Hogg, A.G., Hughen, K.A., Kaiser, K.F., Kromer, B., Manning, S.W., Niu, M., Reimer, R.W., Richards, D.A., Scott, E.M., Southon, J.R., Staff, R.A., Turney, C.S.M., van der Plicht, J., 2013. IntCal13 and Marine13 Radiocarbon Age Calibration Curves 0-50,000 Years Cal BP.

Riegl, B.M. and Purkis, S.J., 2012. Dynamics of Gulf Coral Communities: Observations and Models from the World's Hottest Coral Sea, in B.M. Riegl and S.J. Purkis (eds.), Coral Reefs of the Gulf: Adaptation to Climatic Extremes, Coral Reefs of the World 3, 71-93, DOI 10.1007/978-94-007-3008-3_5.

Rivers, J., Engel, M., Dalrymple, R., Yuosif, R., Strohmenger, C.J. and Al-Shaikh, I. (2020). Are carbonate barrier islands mobile? Insights from a mid to late-Holocene system, Al Ruwais, northern Qatar. Sedimentology (2020) 67, 534–558, doi: 10.1111/sed.12653.

Roy, K. and Peltier, W.R. (2015). Glacial isostatic adjustment, relative sea level history and mantle viscosity: reconciling relative sea level model predictions for the U.S. East coast with geological constraints. Geophys. J. Int. 201, 1156-1181, doi: 10.1093/gji/ggv066.

Roy, K. and Peltier, W.R. (2017). Space-geodetic and water level gauge constraints on continental uplift and tilting over North America: regional convergence of the ICE-6G C (VM5a/VM6) models. Geophys. J. Int. 210, 1115-1142, doi: 10.1093/gji/ggx156.

Schlager, W. (2004). Fractal nature of stratigraphic sequences. Geology 32, 185-188, doi: 10.1130/G20253.1.

Shinn, E.A., 2011. Interplay between Holocene sedimentation and diagenesis, and implications for hydrocarbon exploitation: return to the sabkha of Ras Umm. Int. Assoc. Sedimentol. Spec. Publ. 43, 133-148.

Southon, J., Kashgarian, M., Fontugne, M., Metivier, B., Yim, W.W.-S., 2002. Marine reservoir corrections for the Indian Ocean and Southeast Asia. Radiocarbon 44 (1), 167-180.

Spada, G. and Melini, D. (2019). On Some Properties of the Glacial Isostatic Adjustment Fingerprints.Water 11, 1844, doi:10.3390/w11091844.

Stern, R.J. and Johnson, P. (2010). Continental lithosphere of the Arabian Plate: A geologic, petrologic, and geophysical synthesis. Earth-Science Reviews 101, 29-67, doi:10.1016/j.earscirev.2010.01.002.

Strohmenger, C., Al-Mansoori, A., Al-Jeelani, O., Al-Shamry, A., Al-Hosani, I., Al-Mehsin, K. and Shebl, H. (2010). The sabkha sequence at Mussafah Channel (Abu Dhabi, United Arab Emirates): Facies stacking patterns, microbial-mediated dolomite and evaporite overprint. GeoArabia, 15, 49-90.

Strohmenger, C.J., Shebl, H., Al-Mansoori, A., Al-Mehsin, K., Al-Jeelani, O., Al-Hosani, I., Al-Shamry, A., Al-Baker, S., 2011. Facies stacking patterns in a modern arid environment: a case study of the Abu Dhabi sabhka in the vicinity of Al-Qanatir Island, United Arab Emirates. I*nt. Assoc. Sedimentol. Spec. Publ*. 43, 149-182.

Suarez-Gonzales, P., Benito, M.I., Quijda, I.E. Campos-Soto, S. (2019). 'Trapping and binding': A review of the factors controlling the development of fossil agglutinated microbialites and their distribution in space and time. *Earth-Science Reviews* 194, 182-215, https://doi.org/10.1016/j.earscirev.2019.05.007.

Williams, H.D., Burgess, P.M., Wright, V.P., Della Porta, G., Granjeon, D. (2011). Investigating carbonate platform types: multiple controls and a continuum of geometries. Journal of Sedimentary Research, 2011, v. 81, 18–37, DOI: 10.2110/jsr.2011.6.

Woodroffe, S.A. and Horton, B.P., 2005. Holocene sea-level changes in the Indo-Pacific. Journal of Asian Earth Sciences 25, 29–43, doi:10.1016/j.jseaes.2004.01.009

Burchette, T.P. and Wright, V.P.,1992. Carbonate ramp depositional systems. Sedimentary Geology 79, 3-57.

Wright, V.P. and Burgess, P.M. (2005). The carbonate factory continuum, facies mosaics and microfacies: an appraisal of some of the key concepts underpinning carbonate sedimentology. Facies 51, 17-23, DOI 10.1007/s10347-005-0049-6.

Quaternary carbonate and evaporite sedimentary facies and their ancient analogues